The Effect of Annealing Temperature on the Microstructure and Properties of Cr–C–Al Coatings on Zircaloy-4 for Accident-Tolerant Fuel (ATF) Applications

Chongchong Tang *, Martin Steinbrück [ID], Mirco Grosse [ID], Sven Ulrich and Michael Stüber

Institute for Applied Materials (IAM-AWP), Karlsruhe Institute of Technology (KIT), Eggenstein-Leopoldshafen, 76344 Karlsruhe, Germany; martin.steinbrueck@kit.edu (M.S.); mirco.grosse@kit.edu (M.G.); sven.ulrich@kit.edu (S.U.); michael.stueber@kit.edu (M.S.)
* Correspondence: chongchong.tang@kit.edu

Abstract: Elemental Cr/C/Al multilayers (stoichiometric ratio: 2:1:1) with and without a Cr overlayer have been synthesized on Zircaloy-4 substrates by magnetron sputtering. The effects of annealing temperatures (400 and 550 °C) on phase/microstructure formation, mechanical properties, and oxidation/corrosion performance have been comparatively studied. Annealing of the multilayers at 400 °C led to the formation of nanocrystalline composite consisting of intermetallic and binary carbide phases. Single-phase Cr_2AlC was obtained after 550 °C annealing, but with microcracking of the coatings. Both annealed coatings displayed similar mechanical properties, high-temperature oxidation, and hydrothermal corrosion mechanisms. The composite coatings annealed at 400 °C significantly enhance the high-temperature oxidation resistance (α-Al_2O_3 scale growth) and hydrothermal corrosion (Cr_2O_3 passivation layer formation) of a Zircaloy-4 substrate without coating microcracking and delamination. Nanocomposite CrCAl-based coatings are promising candidates for coated ATF applications with acceptable processing temperatures and excellent oxidation/corrosion resistances for a zirconium alloy substrate.

Keywords: accident tolerant fuel (ATF); CrCAl coating; thermal annealing; mechanical properties; oxidation and corrosion

1. Introduction

The loss of reactor core cooling at the Fukushima Daiichi Nuclear Power Plant in 2011 eventually led to hydrogen denotation, core meltdown, and release of radioactive contamination, revealing the weaknesses of current zirconium alloy fuel cladding under design extension conditions with severe exothermic oxidation and mechanical degradation [1,2]. Innovative accident-tolerant fuels (ATF) cladding for light water reactors (LWRs), to replace existing zirconium-based alloy cladding, are being intensively pursued worldwide [3,4]. The novel ATF claddings mainly comprise three solutions: coated zirconium alloys, FeCrAl alloys, and SiC_f/SiC composites. Deposition of robust, anti-oxidation coatings on the outer surface of zirconium-based alloy fuel claddings represents one short-term ATF strategy [5,6]. This strategy offers the advantages of maintaining the favorable neutronic and irradiation properties of the zirconium alloy cladding underneath, and the fact that the technological and licensing processes can be easily adopted.

A variety of materials have been evaluated and qualified as coatings on Zr-based alloys in terms of high-temperature oxidation and hydrothermal corrosion for coated ATF applications. Pure Cr and Cr-based coatings represent the most attractive and promising concepts since the Cr_2O_3 scale shows good thermodynamic stability and a low growth rate under both oxidation and hydrothermal corrosion conditions [7–10]. Deposition of pure Cr metallic coatings on full-length cladding tubes by physical vapor deposition (PVD) has proven feasible. Lead fuel rods (LFR) with Cr-coated cladding tubes have been inserted and

irradiated in commercial reactors, and the preliminary results promise excellent corrosion and irradiation performances from pure Cr coatings [11,12]. However, some limitations still exist for pure metallic Cr coatings, for instance the eutectic reaction between Cr and Zr at ~1330 °C and the potential formation of volatile species at temperatures above 1200 °C [13,14]. It is well known that an alumina scale can provide better high-temperature oxidation resistance than a chromium oxide scale because of the lower growth kinetics and negligible volatilization rate [15]. Compared to pure Cr, Cr–Al compounds could provide better oxidation resistance through the growth of an alumina-rich or pure alumina scale [16,17]. In addition, the incorporation of carbon into the metallic coating system could mitigate the harmful eutectic reaction between coating and substrate, considering the refractory nature of transition metal carbides [18]. Therefore, materials in the ternary Cr–C–Al system offer promising potential to overcome the aforementioned drawbacks of pure metallic Cr coatings for ATF applications.

One particular material in the Cr–C–Al system that has recently attracted great attention for coated ATF applications is the Cr_2AlC MAX phase. MAX phases ($M_{n+1}AX_n$ phases, a combination of early transition metal (M), A-group element (A), and C or N (X), n typical 1–3) are a family of nanolaminated ternary compounds [19,20]. These materials have a specific hexagonal crystal structure with different $M_{n+1}X_n$ layers interleaved with pure A-element monolayers. The M–X bonding has a strong covalent nature, while the M–A bonding is more of the metallic type and weaker. The unique layered structure and bonding characteristics give these ternary compounds a combination of metallic and ceramic properties. In general, MAX phases are lightweight, relatively soft, readily machinable, and electrically and thermally conductive, and show higher fracture toughness and damage tolerance compared to most ceramics [21]. Several Al-containing MAX phase carbides (for instance, Ti_2AlC, Cr_2AlC, and Ti_3AlC_2) can form a dense protective alumina scale during high-temperature oxidation, which makes them promising candidates for application in harsh environments [22]. Cr_2AlC MAX phase thin films/coatings on zirconium-based alloy have been successfully synthesized by various PVD techniques recently, and their selected properties, for instance high-temperature oxidation, hydrothermal corrosion, and irradiation behavior, have been occasionally studied [23–27]. It has been reported that Cr_2AlC coatings have excellent oxidation and corrosion resistance, as well as good mechanical and radiation stability. However, some challenges still exist for ATF applications, particularly the relatively high processing temperatures [28,29] and frequently reported coating microcracking due to the large thermal expansion coefficient mismatch between the coating and the substrate [24,30].

In this study, magnetron-sputtered Cr/C/Al elemental multilayers (with or without a Cr overlayer) of a chemical composition corresponding to Cr_2AlC stoichiometry have been deposited on Zircaloy-4 substrates. Different thermal annealing conditions have been explored to examine the effects of annealing parameters on their phase/microstructure formation, mechanical properties, and oxidation/corrosion performance. The results show that annealing of the multilayered films below the crystallization onset temperature of Cr_2AlC MAX phase and at typical stress-relief annealing (SRA) temperature (~400 °C [31,32]) of Zircaloy cladding tubes can avoid coating microcracking and microstructure/mechanical property modification of the substrate. The findings herein provide important guidance for optimizing the deposition/processing conditions and associated microstructure and properties of CrCAl-based coatings on zirconium alloy cladding for ATF applications.

2. Materials and Methods

Commercial Zircaloy-4 plates (10 mm × 10 mm or 10 mm × 15 mm, thickness ~0.6 mm) were used as substrates for coating deposition in this study. The chemical composition of the Zircaloy-4 substrate is Sn ~1.4, Fe ~0.22, Cr ~0.10, O ~1000 ppm, Zr bal (wt.%). The plates were polished using SiC sandpaper with a finished surface roughness (Ra) of ~50 nm. The as-deposited coatings comprise two different designs, i.e., a CrCAl coating and a Cr-top-coated Cr/CrCAl coating. The CrCAl layer consists of periodical, elemental Cr/C/Al

multilayered stacks in both designs, which are schematically depicted in Figure 1. The thicknesses of each individual elemental layer were calculated based on the stoichiometric ratio (i.e., 2:1:1) of Cr_2AlC MAX phase: ~7 nm for Cr, 2 nm for C (graphite), and 4 nm for Al. In the first design, multilayered stacks were repeated until the thickness reached ~6 µm. In the second design, the thickness of the multilayered stacks was decreased to ~4.5 µm. Afterwards, an unalloyed, ~1.5-µm-thick Cr layer was deposited on top. The Cr overlayer is intended to avoid possible rapid hydrothermal dissolution of Al during reactor normal operations and potentially enhances coating mechanical properties. Both designs apply a thin Cr interlayer (500 nm), initially on the Zircaloy-4 substrate, to improve the coating adherence. The final thickness was around 6.5 µm for both coating designs. The coatings were deposited using laboratory PVD equipment (Leybold Z 550 coater, Cologne, Germany) from three element targets, i.e., chromium, graphite, and aluminum. The vacuum chamber was evacuated to a pressure of approximately 1×10^{-4} Pa before deposition. The substrates were plasma-etched with a RF (radio frequency) power of 500 W and 0.5 Pa Ar for 15 min. During deposition, the Ar working pressure was maintained at 0.5 Pa and the power was 200 W for all three targets, with RF for Cr and Al and DC (direct current) for C. The Zircaloy-4 substrates were grounded and not heated during deposition. The Cr bonding layer and overlayer were deposited by only switching on the power of the Cr target. The Cr/C/Al multilayered stacks were realized by steering the sample holder and shutter movement. The thickness of each elemental layer was controlled by defining the sample holding times at each individual target position based on individual deposition rates. More detailed descriptions on coating deposition can be found in previous publications [33,34].
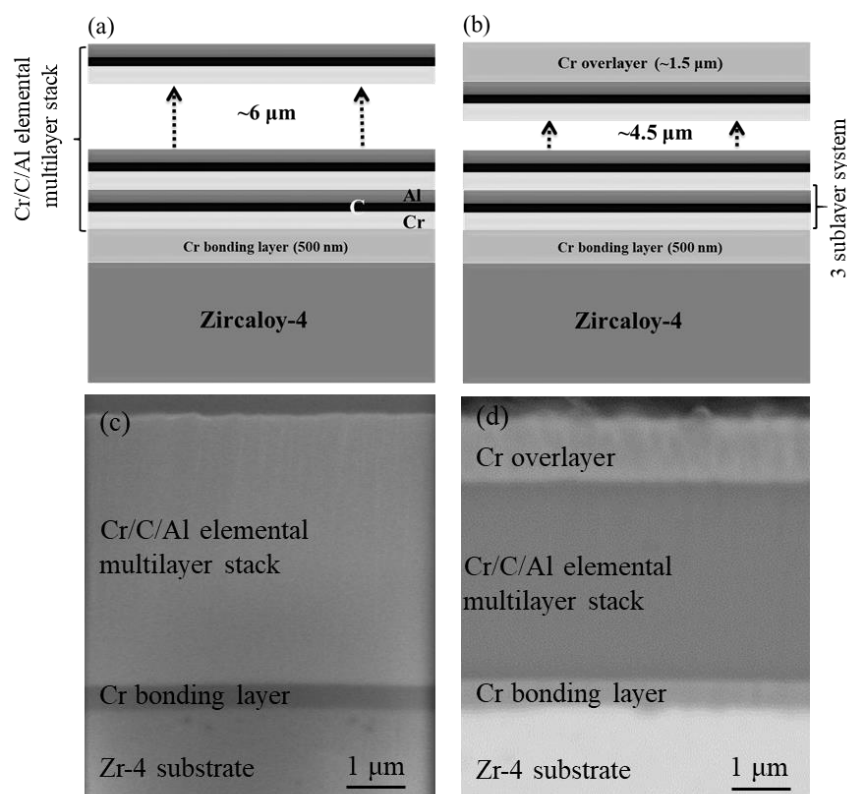

Figure 1. Schematic illustrations and SEM cross-sectional images showing the two designs of coatings on Zircaloy-4 substrate. (**a**,**c**) CrCAl-coated, (**b**,**d**) Cr/CrCAl-coated [30]. Please note that the Cr bonding layer was omitted in the sample identifications. In the second design, the first Cr represents the surface Cr overlayer.

After deposition, the as-deposited coatings were thermally annealed at two different temperatures, i.e., 400 and 550 °C, for 4 h at atmospheric pressure in argon using the furnace of a thermal analyzer (NETZSCH STA-449 F3 Jupiter, Selb, Germany). The selection of

these two annealing temperatures was based on two considerations: (1) acceptable processing temperature for Zircaloy substrate and (2) phase transition of the coating materials. The annealing temperature of 400 °C represents a typical stress-relief annealing (SRA) temperature during the fabrication of Zircaloy cladding tubes, which will not affect the microstructure and mechanical properties of the substrate [31]. Our previous studies have confirmed that crystallization of Cr_2AlC from the multilayered stacks is at ~480 °C [33]; annealing at the two different temperatures will thus result in different phase formation. Annealing at 400 °C will lead to the formation of binary compounds. The higher annealing temperature of 550 °C can promote Cr_2AlC MAX phase formation via a solid-state diffusion reaction from the Cr/C/Al multilayered stacks. The phase and microstructure formation, mechanical properties, and oxidation/hydrothermal corrosion resistance of the coatings, after annealing at the two different temperatures, were investigated to compare their performance and select the suitable annealing conditions for further optimizing the coatings.

The phase constitution of both as-deposited and annealed coatings were identified by X-ray diffraction (XRD, Seifert PAD II diffractometer, Richard Seifert & Co., Ahrensburg, Germany) with θ–2θ scans using CuKα radiation (λ = 1.54 Å) at 40 kV and 30 mA. The surface and cross-sectional microstructure of selected samples were examined by scanning electron microscopy (SEM, PhilipsXL30S, Eindhoven, Netherlands). Microindentation and scratch tests were performed to evaluate the mechanical properties and adherence of the annealed coatings. The microindentation tests were carried out using a CSM Micro Kombi Tester (Anton Paar, Graz, Austria) with a Vickers diamond tip. The indentation depth was adjusted to be lower than 1/8 of the total film thickness to avoid substrate effect. The indentations were repeated 12 times and the results were analyzed according to the method introduced by Oliver and Pharr [35,36]. The scratch tests were done using a CSM Micro Kombi Tester with a diamond Rockwell tip of 200 μm diameter and a normal load range of 0 to 30 N at a velocity of 10 mm/min. Five scratch tests were implemented on each sample. The failure type and average critical loads of failure were evaluated by inspecting the optical/SEM micrographs of the scratches.

High-temperature oxidation tests and quench tests in steam were performed using a NETZSCH thermal balance with a water vapor furnace and a horizontal alumina furnace (BOX) [13], respectively. In the case of tests in thermal balance, the samples were heated to the predefined temperature at a heating rate of 20 K/min in argon. Steam was subsequently injected directly into the reaction tube from the top produced by a steam generator (steam flow 2 g/h). In the quench tests, the coated samples were oxidized in steam at 1000 °C for 30 min. Then the samples were quickly pulled out and quenched in water (room temperature, ~25 °C). The quenched samples were re-oxidized in steam at 1000 °C for 1 h using the thermal balance to check their protection after quenching. The hydrothermal corrosion behavior of the uncoated and two coated Zircaloy-4 (400 °C-annealed) samples were studied by autoclave tests. The tests were done using a static autoclave with 1000 ppm B and 2 ppm Li at ~330 °C and 18 MPa for 30 days (pressurized water reactor conditions, static autoclave, SCK·CEN, Mol, Belgium). After the oxidation and hydrothermal corrosion tests, the oxide scale growth, morphology, and microstructure of the samples were examined by XRD and SEM.

3. Results

3.1. Microstructure and Phase Formation

Figure 2 displays the surface morphology of the coated Zircaloy-4 in the as-deposited state, and after annealing at 400 and 550 °C for 4 h in argon, respectively. Both the as-deposited and 400 °C-annealed coatings revealed a smooth surface topography without recognizable microcracking and macroscale defects. However, after annealing at 550 °C, both coatings showed microcracking on the surface, as shown in Figure 2c,f. The cracking of the coatings was consistent with our previous study on identical coatings after annealing at 550 °C for only 10 min [30]. All coatings showed good adherence without delamination

or spallation. The cross-sectional images of the coatings shown in Figure 1c,d display their dense microstructure. The Cr bonding layer/overlayer and the elemental Cr/C/Al multilayered stacks can be straightforwardly distinguished by their different contrast.
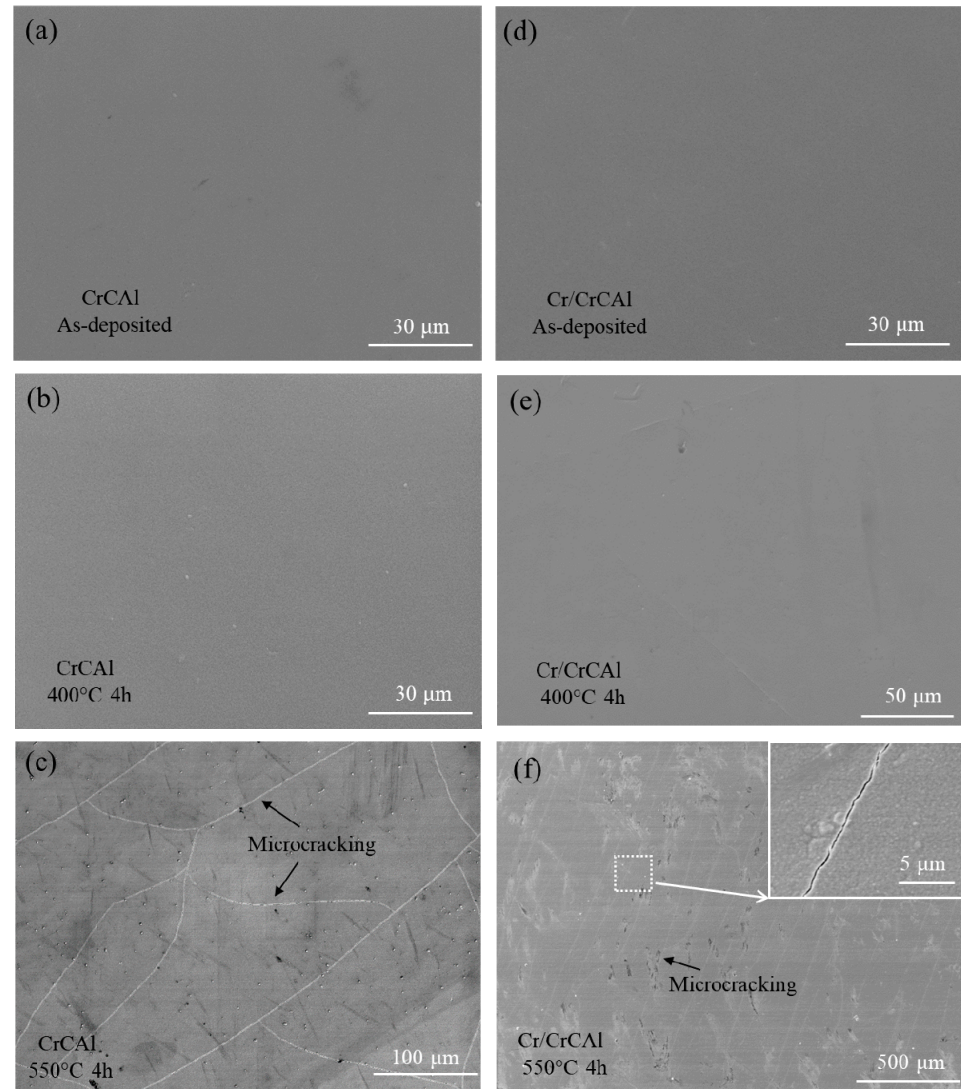

Figure 2. Surface appearance of as-deposited, 400 °C- and 550 °C-annealed coatings. (**a–c**) CrCAl-coated; (**d–f**) Cr/CrCAl-coated.

Figure 3 shows the XRD patterns of the as-deposited, 400 °C- and 550 °C-annealed coated Zircaloy-4. The diffraction peaks marked with Zr (JCPDS card 05-0665) all originate from the Zircaloy-4 substrate. The as-deposited coatings are composed of nanocrystalline metallic layers and amorphous carbon layers. In the case of CrCAl-coated Zircaloy-4, only one Cr(110) diffraction signal was detected for the Cr phase in the as-deposited state. In comparison, two diffraction peaks, Cr (110) and Cr (200), were seen for the Cr/CrCAl-coated Zircaloy-4. These observations indicate that the Cr nanolayers have a (110) preferred orientation in the multilayered CrCAl stacks, while the thick Cr overlayer grows with more randomly oriented grains. After annealing at 400 °C, only one broad diffraction hump with a relatively low intensity was recorded, centered roughly at 44°, apart from the Zr peaks for the CrCAl-coated samples. The results suggest that the elemental Cr/C/Al multilayered stacks transformed into a nanocrystalline composite consisting of binary carbide and intermetallic phases. Our previous investigations have proved that the crystallization onset temperature for Cr_2AlC MAX phase during annealing such

multilayered stacks is approximately 480 °C and binary compounds formed at intermediate annealing temperatures before the crystallization of specific MAX phase [33,37]. The results here are consistent with our previous findings. The possible phase constitutions after annealing at 400 °C are Cr_7C_3 (JCPDS card 34-1682) and Cr_8Al_5 (JCPDS card 29-0015) by comparing with standard JCPDS cards. However, their poor crystallinity, designated by only a few diffraction peaks, makes it difficult to recognize the specific steps of phase formation. More comprehensive microstructure and phase identifications using advanced methods, such as high-resolution transmission electron microscopy (HRTEM), are ongoing. Formation of a phase-pure and basal-plane textured Cr_2AlC MAX phase from the elemental Cr/C/Al multilayered stacks was observed after annealing at 550 °C for the CrCAl-coated samples [33]. The Cr (110) signal originates from the Cr bonding layer beneath. In the case of the Cr/CrCAl coatings, similar phase formations were seen after annealing at the two different temperatures, except the existence of the Cr overlayer reduced the intensity of the diffraction signal from the CrCAl multilayered stacks. Since no cracks were observed for the 400 °C-annealed coatings, it can be concluded that the main reason for the microcracking of 550 °C-annealed coatings is the formation of Cr_2AlC MAX phase, which has a considerably higher thermal expansion coefficient (11–13.3 $\times$ 10^{-6} K^{-1}) compared to the Zircaloy-4 substrate (~6 $\times$ 10^{-6} K^{-1}) [30].
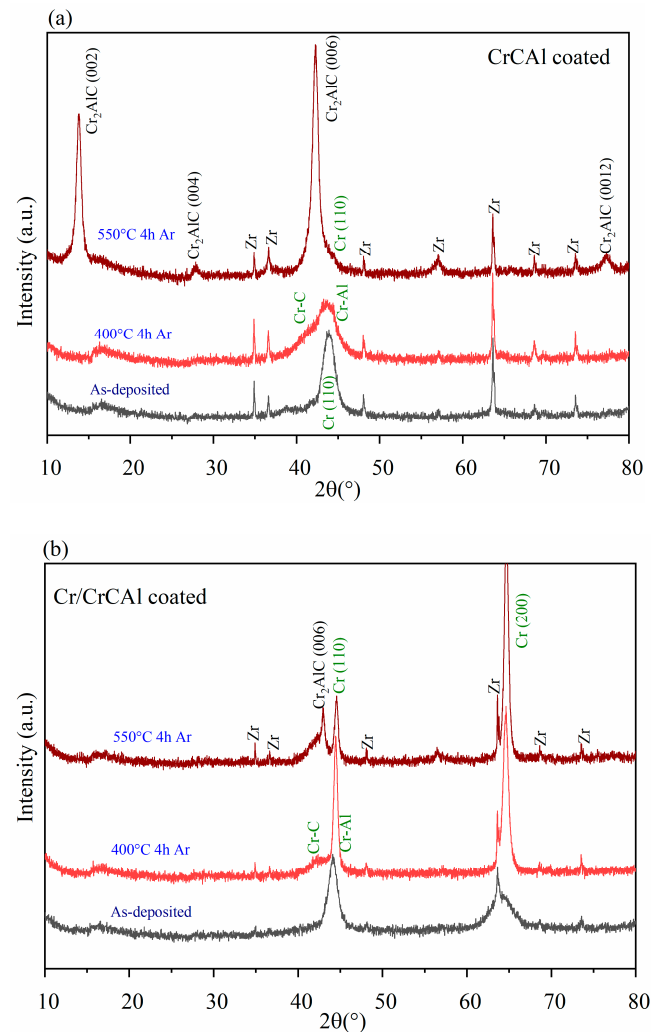

Figure 3. XRD patterns of as-deposited, 400 °C- and 550 °C-annealed coated Zircaloy-4. (**a**) CrCAl-coated and (**b**) Cr/CrCAl-coated.

3.2. Microindentation and Scratch Test

Table 1 shows the hardness and reduced Young's modulus of the coatings after annealing at the two different temperatures measured by microindentation. The experimental and theoretical values of hardness and modulus of relevant bulk materials in this coating–substrate system are also included for comparison. The H/E* ratios, which represent a convenient empirical parameter to evaluate a coating's toughness, were calculated and included. In general, coatings with H/E* > 0.1 are tough and more resistant to cracking, while coatings with H/E* ≤ 0.1 are brittle and less elastic [38]. The two coatings display very similar values of hardness and modulus after annealing at the same temperature, i.e., 400 and 550 °C. The hardness and modulus values increase slightly after 550 °C annealing. The hardness and Young's modulus for Zirclaoy-4 substrate, bulk Cr, and Cr_2AlC show comparable values except for the intermetallic compound Cr_2Al. This can be anticipated since intermetallic compounds are generally brittle with a low fracture toughness. In comparison, the coatings display much higher values, i.e., ~13 GPa hardness and 200 GPa modulus, similar to Cr_2Al. The much higher hardness value of Cr_2AlC coating than bulk Cr_2AlC can be attributed to its nanosized grains and growth defects. In addition, their H/E* ratios are very close, but obviously lower than 0.1. The above observations reveal their more stiff and brittle nature compared to the Zircaloy-4 substrate.

Table 1. Hardness and reduced Young's modulus of the coatings determined by microindentation.

ID.	Hardness (H, GPa)	Young's Modulus (E*, GPa)	H/E*
CrCAl 400 °C 4 h	11.3 ± 0.3	179.4 ± 4.0	0.063
CrCAl 550 °C 4 h	14.1 ± 0.5	212.0 ± 8.1	0.067
Cr/CrCAl 400 °C 4 h	12.2 ± 0.4	189.2 ± 8.3	0.064
Cr/CrCAl 550 °C 4 h	13.7 ± 0.3	219.6 ± 10.3	0.063
Zr [34]	2.8	99.3	-
Cr [12]	~2.7	130	-
Cr_2Al [16]	13.6	180.7	-
Cr_2AlC [19]	~5.2	193	-

Figure 4 gives scanning electron micrographs of typical scratch tracks for the two types of coatings annealed at 400 and 550 °C. All coatings displayed brittle failure modes, with tensile cracking at low applied load and chipping/delamination at high load. This failure behavior represents a common failure mode for hard coatings on ductile substrates [39]. The critical failure load (L_c) was defined as the value at which coating chipping occurred and the uncovered substrate was regularly visible along the scratch track. The average critical failure loads based on five scratches were 15.2 and 22.5 N for CrCAl 25.2 and 27.3 N for Cr/CrCAl, annealed at 400 and 550 °C, respectively. Addition of a metallic Cr overlayer obviously enhances the coating's resistance to cracking and spallation. In addition, the higher annealing temperature (550 °C here) also improves the coating adherence, with higher critical failure loads owing to enhanced interdiffusion. It is necessary to point out that all coatings showed good interfacial strength since chipping/delamination of the coatings was only seen at relatively higher loads.
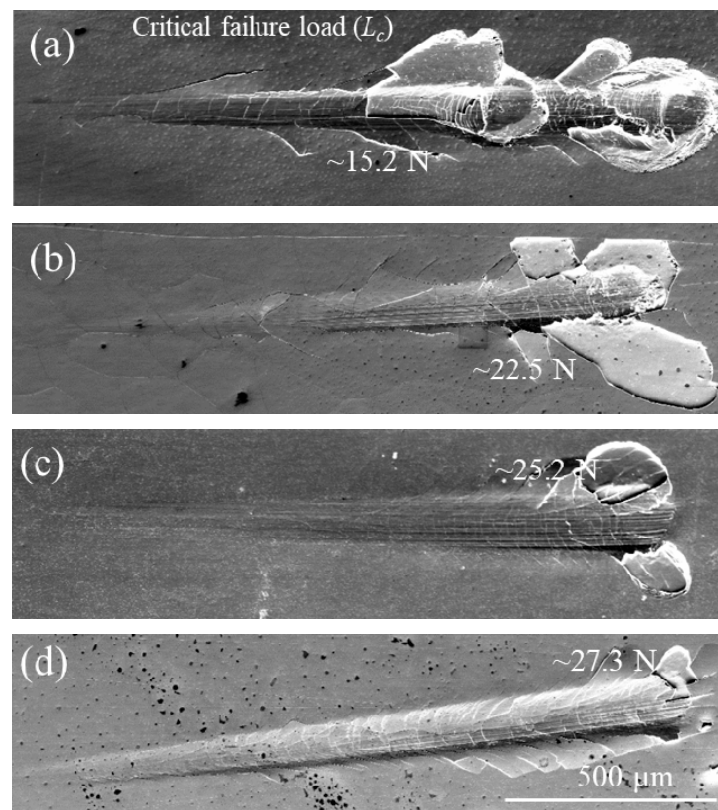
Figure 4. Scanning electron micrographs of typical scratches on the different coated samples. (**a**) 400 °C- and (**b**) 550 °C-annealed CrCAl, (**c**) 400 °C- and (**d**) 550 °C-annealed Cr/CrAl. The average critical failure loads for each sample are also marked in the images.

3.3. Oxidation and Quench Test

Intensive high-temperature oxidation tests in steam were conducted to understand the oxidation mechanisms and failure behavior of the two types of coatings. The obtained results indicate that each type of coating revealed the same oxidation mechanism at high temperatures, irrespective of annealing temperatures. More specifically, a dense, single-layer Al_2O_3 formed on the CrCAl-coated samples during high-temperature oxidation. Oxidation of the Cr/CrCAl-coated ones resulted in the growth of a bilayer oxide scale with an outer Cr_2O_3 layer and an inner Al_2O_3 layer [30]. These phenomena can be explained by the fact that the CrCAl multilayered stacks can rapidly transform to the Cr_2AlC MAX phase during the heating period starting from ~480 °C [33]. Oxidation of Cr_2AlC proceeds with selective oxidation of Al, leading to the growth of an alumina scale.

Figures 5 and 6 show the oxidation performance of 400 °C-annealed samples with a transient test from 300 to 1000 °C in steam and subsequent 10 min holding time at 1000 °C. As seen in Figure 5a, oxidation of both coated samples demonstrated one order of magnitude lower mass gain compared to the uncoated one. The mass gains were very similar for the two-coated samples, which proves their excellent oxidation resistance in steam. XRD analysis confirmed that the main phase within the CrCAl coating was now the Cr_2AlC MAX phase, highlighted by its high intensity and narrow diffraction peaks. The findings here prove that the CrCAl multilayered stacks transform into the Cr_2AlC MAX phase during the heating period, accompanied by grain growth and aggregation. The alumina and binary chromium carbide phases are reaction products owing to selective oxidation of Al. In the case of the Cr/CrCAl-coated samples, oxidation of the Cr overlayer resulted in the formation of the Cr_2O_3 phase, which represented the main phase detected by XRD. Due to the limited X-ray detection depth, the surface Cr_2O_3 layer and unoxidized Cr layer block the information inside the coating.
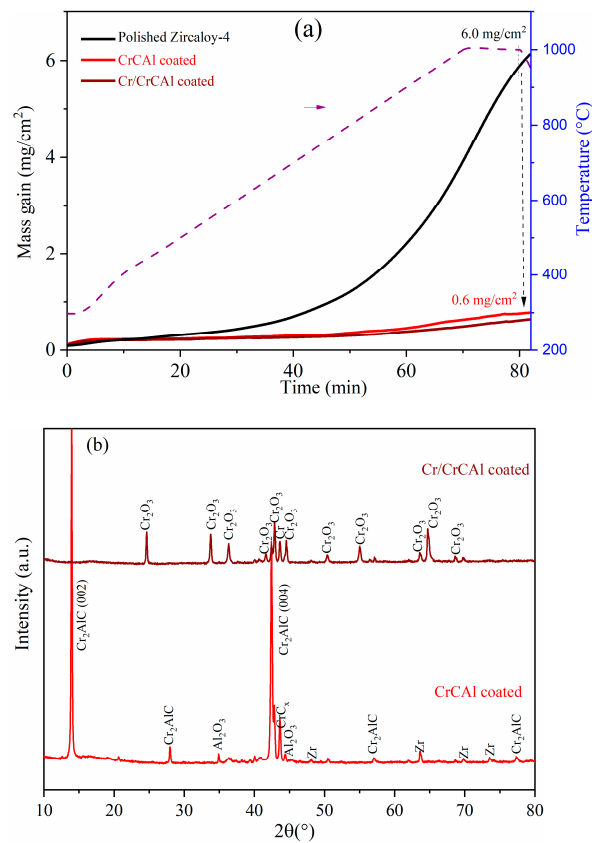
Figure 5. Oxidation behavior of 400 °C-annealed samples with transient test from 300 to 1000 °C with 10 min holding at 1000 °C in steam. (**a**) Mass gain during the test; (**b**) phase identification by XRD after test.
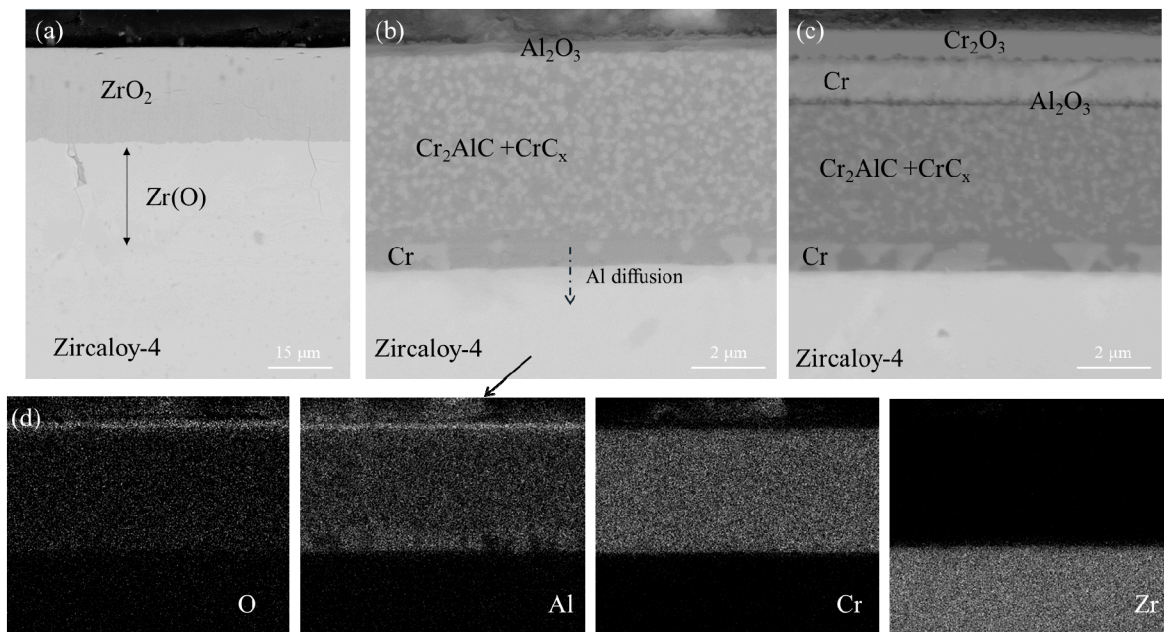

Figure 6. SEM-BSE cross-sectional images showing the oxide scale configurations after transient oxidation test from 300 to 1000 °C on uncoated and coated Zircaloy-4. (**a**) Uncoated; (**b**) CrCAl-coated; (**c**) Cr/CrCAl-coated; (**d**) EDS mapping results of CrCAl-coated sample.

The different oxide scale configurations on the three samples can be easily seen from the SEM cross-sectional images in Figure 6. Oxidation of the uncoated Zircaloy-4 resulted in the formation of a relatively thick ZrO_2 layer on top and an oxygen-stabilized $Zr(O)$ layer beneath. The thicknesses of the ZrO_2 and $Zr(O)$ layer were ~23.5 and 25.7 μm, respectively. In comparison, a very thin and dense alumina layer (~0.3 μm thick) grew on the CrCAl-coated sample. Selective oxidation of Al from the coating causes the Cr_2AlC to partially decompose into binary chromium carbides [40]. With respect to the Cr/CrCAl-coated sample, the Cr overlayer was not completely oxidized, a ~1.1 μm thick Cr_2O_3 layer formed on the surface. In addition, inward diffusion of oxidants, mainly through columnar grain boundaries of the Cr overlayer, led to the growth of a thin alumina layer at the Cr/CrCAl interface. Inward diffusion of Al from the coatings through the Cr bonding layer into the Zircaloy-4 substrate after oxidation was seen for both coatings by EDS measurement.

Quench tests after oxidation at 1000 °C for 30 min in steam were done to check the coating adherence during thermal shock conditions, the results are given in Figure 7. The two-coated samples displayed different surface colors due to different oxide scale formations on the surface (i.e., alumina and chromia, respectively). Both coatings survived without large area spallation or delamination after quenching, except for some localized coating spallation adjacent to the suspension hole. Microcracking of both coatings after quenching was seen on the surface by SEM (not shown here). The localized coating spallation near the suspension hole was most probably due to the intensive oxidation of the uncoated substrate and stress concentration. Overall, both coatings demonstrated high adherence at high temperatures and can tolerate harsh thermal shock conditions if no macroscale pre-defects exist.
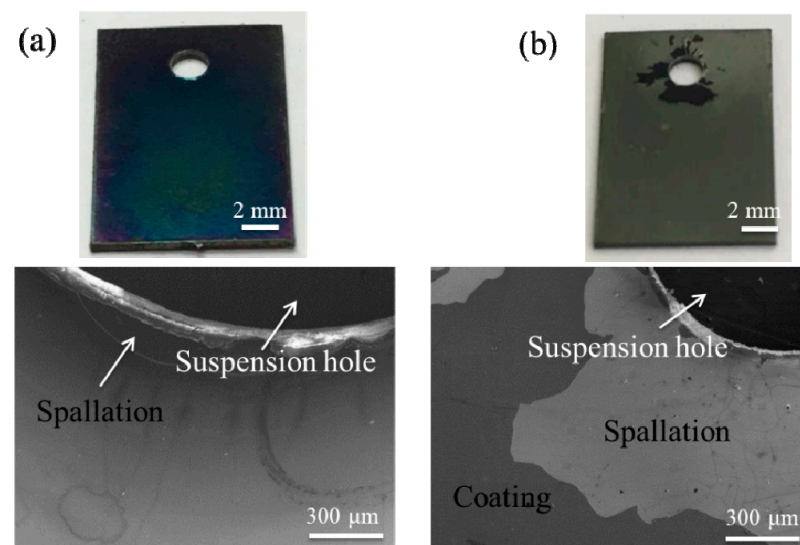

Figure 7. Post-quench surface appearances and SEM images of the two-coated samples. (**a**) CrCAl-coated; (**b**) Cr/CrCAl-coated.

The quenched samples were re-oxidized at 1000 °C for 1 h in steam to check their protective performance; one example of results of the CrCAl-coated sample is shown in Figure 8. The localized coating spallation and oxidation of the uncoated substrate around the suspension hole caused coating failure via macrocracking and delamination. Strong oxidation of the substrate in uncoated edges and coating failure areas was confirmed, and the failure areas gradually expanded to the center region of the samples. However, the failure areas were only within the range of ~2 mm around the suspension hole and the coating still displayed protective behavior in other regions. Similar to before, a thin and dense alumina scale grew on the surface, which protected the coating and substrate from oxidation. In addition, the quench-induced surface cracks were self-healed by alumina growth and there were no signs of oxidation of the Zircaloy-4 substrate in the regions

where the coating was still protective. Overall, the local spallation of the coatings has a limited impact during high-temperature oxidation without catastrophic failure of the coating–substrate system.
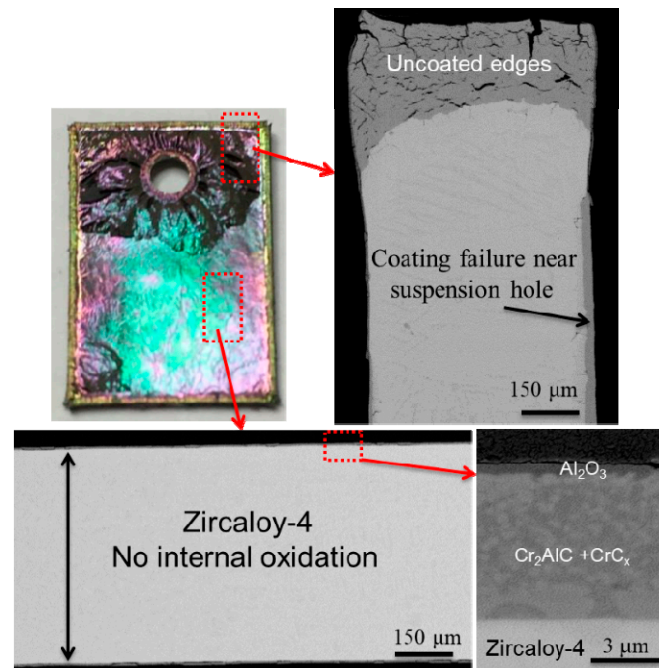

Figure 8. Surface appearances and cross-sectional SEM images of CrCAl-coated Zircaloy-4 oxidized at 1000 °C for 1 h after quenching.

3.4. Autoclave Test

Protective coatings on zirconium alloy for ATF applications ought to have excellent hydrothermal corrosion resistance and endure long-term in-pile operating conditions. Microcracking was seen on 550 °C-annealed coatings and our previous short-term autoclave tests found premature failure of these coatings due to inward diffusion of water and hydrothermal corrosion of Zircaloy-4 substrate beneath the cracks [30]. Therefore, only samples annealed at 400 °C were exposed to a relatively long-term 30-day autoclave test to examine their hydrothermal corrosion resistance. The surface appearance and cross-sectional structure of these samples after the autoclave tests are shown in Figure 9. The mass changes after the autoclave tests for uncoated, CrCAl-coated and Cr/CrCAl-coated Zircaloy-4 were 0.3, 0.3, and −0.5 mg, respectively. The CrCAl coatings revealed excellent adherence without any delamination or spallation, as seen in Figure 9a. The identical mass gain of uncoated and CrCAl-coated Zircaloy-4 indicated the excellent hydrothermal corrosion resistance of the CrCAl composite coatings. Limited local spallation was found for the Cr/CrCAl coatings near the suspension area (Figure 9b), which caused a small negative mass change. SEM-EDS investigations indicated the growth of a thin Cr_2O_3 layer on the surface of both types of coatings, which guaranteed their excellent hydrothermal corrosion resistance. The coating thicknesses were barely changed with respect to the low growth kinetics of the Cr_2O_3 layer, as shown by the cross-sectional SEM images in Figure 9c,d. Thus, annealing the coatings at 400 °C instead of 550 °C represents a reasonable solution to avoid coating cracking and maintain the coating's excellent oxidation and corrosion resistance.
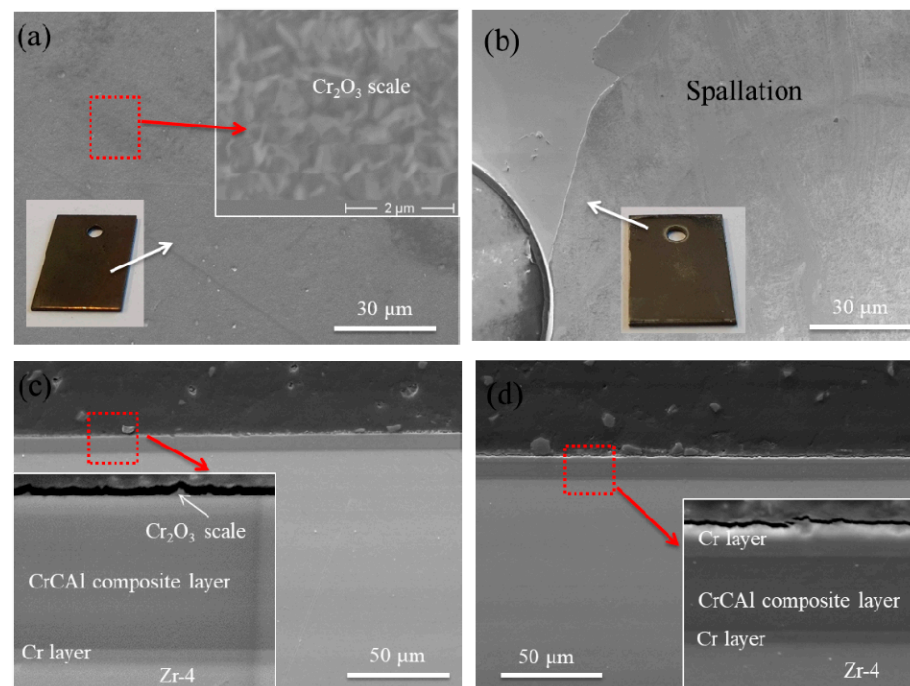
Figure 9. Surface appearances and cross-sectional SEM images of 400 °C-annealed, coated Zircaloy-4 after autoclave test at ~330 °C and 18 MPa for 30 days. (**a**) CrCAl-coated surface; (**b**) Cr/CrCAl-coated surface; (**c**) CrCAl-coated cross section; (**d**) Cr/CrCAl-coated cross section.

4. Discussion

The CrCAl-based coatings represent an attractive concept for the application of coated ATF cladding, because they form passivation Cr_2O_3 scale under nominal conditions (hydrothermal corrosion) and a protective Al_2O_3 scale during accidental scenarios (high-temperature steam oxidation). The lower growth kinetics of Al_2O_3 scale compared to Cr_2O_3 scale during high-temperature oxidation in steam can allow thinner coatings with respect to a pure, metallic Cr coating. Even though there is not much thermodynamic information on such CrCAl-based coatings in contact with the Zircaloy substrate, a carbon-containing ternary system could potentially avoid or mitigate the formation of an unfavorable liquid phase (eutectic reaction) between the coating and substrate at relatively low temperatures.

Our initial research focused on the synthesis of Cr_2AlC MAX phase coatings in this ternary system by thermal annealing of the Cr/C/Al multilayered stacks [30,33]. The Cr_2AlC coatings show excellent hydrothermal corrosion and high-temperature oxidation resistances; however, the coatings undergo microcracking after 550 °C thermal annealing because of the large thermal expansion coefficient mismatch with the substrate. These microcracks can lead to premature failure of the coatings during nominal reactor conditions. In addition, the 550 °C annealing temperature is slightly higher than the typical stress-relief annealing (SRA) temperature (~400 °C) of Zircaloy cladding tubes. These issues could restrict the utilization of Cr_2AlC MAX phase coatings, fabricated by thermal annealing of multilayered/amorphous precursors or directly deposited by PVD at specific temperatures, on Zircaloy-4 for ATF application. Our previous study using in situ high-temperature XRD confirmed that the Cr/C/Al multilayered stacks transform to nanocrystalline composite starting at 420 °C, followed by phase transition at 480 °C with crystallization of the Cr_2AlC MAX phase [33]. The current study found that reducing the annealing temperature to 400 °C and avoiding the formation of Cr_2AlC MAX phase would not cause cracking of these CrCAl-based coatings after annealing. The 400 °C annealing promotes the Cr/C/Al multilayered stacks' transformation to nanocomposite coatings consisting of binary carbide and intermetallic phases. These phases have been frequently reported and are recognized as intermediate phases during the synthesis of the Cr_2AlC MAX phase [41]. In addition,

these binary compounds have been reported to have similar thermal expansion coefficients to the Zircaloy-4 substrate [42], which makes the 400 °C-annealed coatings crack-free. The 400 °C, 4 h annealing condition in argon provides a way to fabricate CrCAl-based coatings on the Zircaloy substrate with an acceptable processing temperature and high quality.

Microindentation and scratch tests found that all annealed coatings showed brittle failure modes at room temperature. It can be anticipated that even a pure metallic Cr coating will show brittle fracture behavior at room temperature during tensile tests [9,43], and the binary carbide/intermetallic and ternary MAX phase coatings are typically elastically stiffer than pure Cr [21]. The 400 °C (with nanocomposite formation) and 550 °C (with Cr_2AlC MAX phase formation) annealed coatings revealed very similar hardness and modulus values. The different phase constitutions do not seem to contribute considerably to their mechanical properties, probably because of their nanocrystalline structure. However, by applying a Cr overlayer, the Cr/CrCAl coatings demonstrated higher resistance to chipping and spallation in scratch test compared to the CrCAl coatings. Multilayered coatings composed of alternating metallic and ceramic layers have been proven to possess enhanced mechanical properties due to interface toughening and hardening [44]. Even though all coatings showed good adherence, as evidenced by a scratch test, coating cracking and delamination/spallation can occur near the regions where the cladding undergoes ballooning and bursts during accidental conditions. The above quenching test found that failure of the coatings may be limited to local areas, and microcracks can be self-healed by selective oxidation of aluminum and the growth of an aluminum oxide scale. However, their mechanical properties and potential mechanically associated failure modes under both normal operations and accidental transient conditions have to be systematically studied.

High-temperature oxidation in steam proved that the coatings annealed at the two different temperatures revealed the same oxidation mechanism. It is foreseeable since oxidations were usually carried out at temperatures above 800 °C, while the crystallization onset temperature of the Cr_2AlC MAX phase from the multilayered stacks is already at ~480 °C. The nanoscale multilayered design of the as-deposited coatings allows for the transition from the binary mesophases to the ternary Cr_2AlC MAX phase within a few minutes at ~500 °C [33]. At temperatures below 500 °C, the coatings are barely oxidized, as seen from the transient tests in Figure 5. Thus, the two annealed coatings will have the same phase composition, i.e., Cr_2AlC for the CrCAl layer, before the temperature reaches the values at which significant oxidation takes place. In the Cr_2AlC MAX phase, the covalent–ionic Cr–C bonds are much stronger than the metallic Cr–Al bonds, which makes the Al atoms highly mobile [19,20]. Previous intensive studies of the high-temperature oxidation of Cr_2AlC have confirmed that selective oxidation of Al occurred, leading to the formation of a protective alumina scale due to its unique bonding characteristics [22,24,29,40]. Oxidation-induced failure of both coatings at high temperatures is mainly due to outward diffusion and depletion of Al, which resulted in the formation of voids, oxidation of Cr and C, and subsequent coating cracking. Relatively long-term oxidation in steam found that both ~6.5-μm coatings could protect the substrate from oxidation for about 120 min at 1000 °C and 30 min at 1200 °C [45]. Increasing the thickness of the CrCAl layer will increase the Al reservoir within the coatings and provide a longer protection period. Previous transient tests up to 1400 °C in steam did not find any sign of eutectic reaction between the coating and substrate [30]. Outward diffusion of Al to form alumina scale essentially leads to binary chromium carbide in contact with the Zircaloy substrate at the interface, which we expect to increase the eutectic reaction temperature. Thermodynamic assessments of the CrCAl–Zr system with experimental and theoretical calculations are needed to better understand the interfacial behavior at high temperatures.

Autoclave tests simulating PWR normal operation conditions for 30 days found that the 400 °C-annealed, nanocomposite coatings demonstrated excellent hydrothermal corrosion resistance via passivation Cr_2O_3 scale formation. No coating spallation and preferential dissolution of Al were seen after the relatively long-term test. It is proposed that the relatively high Cr concentration (50 at.%) within the CrCAl coatings herein stimulates the

formation of a passivation Cr_2O_3 scale under hydrothermal corrosion conditions, irrespective of annealing temperatures. The passivation Cr_2O_3 scale with low growth kinetics protects the coatings from fast hydrothermal corrosion or Al dissolution. The Al reservoir can be preserved to form alumina scale in case of accidents with high-temperature steam or air oxidation. However, it should be pointed out that the autoclave tests were done in static conditions without flowing coolant, cladding fretting, or neutron irradiation. The coating performance under in-pile conditions and the abovementioned harsher environments must be validated in the future.

5. Conclusions

CrCAl-based coatings with two different designs, i.e., a CrCAl coating and a Cr-top-coated Cr/CrCAl coating, have been deposited on a Zircaloy-4 substrate by magnetron sputtering for ATF application. The CrCAl layer consists of periodical, elemental Cr/C/Al multilayered stacks with a chemical composition identical to that of the Cr_2AlC MAX phase in the as-deposited state. Different thermal annealing treatments have been done to examine the effect of annealing parameters on phase/microstructure formation, mechanical properties, high-temperature oxidation, and hydrothermal corrosion performance.

The elemental Cr/C/Al multilayered stacks transformed to nanocomposite coatings (composed of binary carbides and intermetallic phases) and a single Cr_2AlC MAX phase coatings after annealing at 400 and 550 °C for 4 h. The 400 °C-annealed coatings were crack-free, while the 550 °C-annealed coatings exhibited microcracking, caused by the large thermal expansion coefficient mismatch between Cr_2AlC and Zircaloy.

All coatings revealed a brittle nature, were stiffer than the Zircaloy-4 substrate, and displayed brittle failure modes in scratch tests. The Cr/CrCAl coatings showed enhanced resistance to chipping/delamination compared to the CrCAl coatings due to interface hardening and toughening.

Both 400 °C- and 550 °C-annealed coatings presented identical oxidation mechanisms and significantly improved high-temperature oxidation resistance with selective oxidation of Al in the CrCAl layer. The reason for this lies in the transformation of the CrCAl layer into the Cr_2AlC MAX phase during the heating period at temperature of ~480 °C. Thermal shock tests revealed that the coatings have good adherence at high temperature before failure and microcracks can be self-healed by the growth of alumina. Long-term hydrothermal corrosion tests for 30 days found that the 400 °C-annealed coatings possess excellent corrosion resistance with a thin, passivation Cr_2O_3 scale formation.

The results obtained herein suggest that a moderate annealing temperature of 400 °C to induce nanocomposite formation of the Cr/C/Al multilayered stacks can prevent coating microcracking due to Cr_2AlC MAX phase crystallization at higher annealing temperatures. The 400 °C annealing temperature represents the typical stress-relief annealing (SRA) temperature of zirconium alloy cladding tubes and is compatible with current industrial manufacturing processes. Multilayered designs consisting of alternating Cr and CrCAl layers offer more innovative coating designs with tailored/enhanced mechanical and corrosion properties for future development.

Author Contributions: Conceptualization, C.T. and M.S. (Michael Stüber); methodology, C.T.; investigation, C.T.; resources, M.S. (Michael Stüber) and S.U.; data curation, C.T.; writing—original draft preparation, C.T.; writing—review and editing, M.G., M.S. (Martin Steinbrück), S.U. and M.S. (Michael Stüber); funding acquisition, C.T. All authors have read and agreed to the published version of the manuscript.

Institutional Review Board Statement: Not applicable.

Informed Consent Statement: Not applicable.

References

1. Hirano, M.; Yonomoto, T.; Ishigaki, M.; Watanabe, N.; Maruyama, Y.; Sibamoto, Y.; Watanabe, T.; Moriyama, K. Insights from review and analysis of the Fukushima Dai-ichi accident. *J. Nucl. Sci. Technol.* **2012**, *49*, 1–17. [CrossRef]
2. Zinkle, S.J.; Terrani, K.A.; Gehin, J.C.; Ott, L.J.; Snead, L.L. Accident tolerant fuels for LWRs: A perspective. *J. Nucl. Mater.* **2014**, *448*, 374–379. [CrossRef]
3. Terrani, K.A. Accident tolerant fuel cladding development: Promise, status, and challenges. *J. Nucl. Mater.* **2018**, *501*, 13–30. [CrossRef]
4. Yun, D.; Lu, C.; Zhou, Z.; Wu, Y.; Liu, W.; Guo, S.; Shi, T.; Stubbins, J.F. Current state and prospect on the development of advanced nuclear fuel system materials: A review. *Mater. Rep. Energy* **2021**, *1*, 100007. [CrossRef]
5. Tang, C.; Stueber, M.; Seifert, H.J.; Steinbrueck, M. Protective coatings on zirconium-based alloys as accident-tolerant fuel (ATF) claddings. *Corros. Rev.* **2017**, *35*, 141–166. [CrossRef]
6. Kashkarov, E.; Afornu, B.; Sidelev, D.; Krinitcyn, M.; Gouws, V.; Lider, A. Recent Advances in Protective Coatings for Accident Tolerant Zr-Based Fuel Claddings. *Coatings* **2021**, *11*, 557. [CrossRef]
7. Brachet, J.C.; Le Saux, M.; Bischoff, J.; Palancher, H.; Chosson, R.; Pouillier, E.; Guilbert, T.; Urvoy, S.; Nony, G.; Vandenberghe, T.; et al. Evaluation of Equivalent Cladding Reacted parameters of Cr-coated claddings oxidized in steam at 1200 °C in relation with oxygen diffusion/partitioning and post-quench ductility. *J. Nucl. Mater.* **2020**, *533*, 152106. [CrossRef]
8. Brachet, J.C.; Rouesne, E.; Ribis, J.; Guilbert, T.; Urvoy, S.; Nony, G.; Toffolon-Masclet, C.; Le Saux, M.; Chaabane, N.; Palancher, H.; et al. High temperature steam oxidation of chromium-coated zirconium-based alloys: Kinetics and process. *Corros. Sci.* **2020**, *167*, 108537. [CrossRef]
9. Ma, X.; Zhang, W.; Chen, Z.; Yang, D.; Jiang, J.; Song, L. Elastoplastic Deformation and Fracture Behavior of Cr-Coated Zr-4 Alloys for Accident Tolerant Fuel Claddings. *Front. Energy Res.* **2021**, *9*, 655176. [CrossRef]
10. Liu, H.; Feng, Y.; Yao, Y.; Li, B.; Wang, R.; Shi, X.; Li, P.; Shu, J.; Huang, F.; Huang, Q.; et al. Effect of the 345 °C and 16.5 MPa autoclave corrosion on the oxidation behavior of Cr-coated zirconium claddings in the high-temperature steam. *Corros. Sci.* **2021**, *189*, 109608. [CrossRef]
11. Bischoff, J.; Delafoy, C.; Vauglin, C.; Barberis, P.; Roubeyrie, C.; Perche, D.; Duthoo, D.; Schuster, F.; Brachet, J.C.; Schweitzer, E.W.; et al. AREVA NP's enhanced accident-tolerant fuel developments: Focus on Cr-coated M5 cladding. *Nucl. Eng. Technol.* **2018**, *50*, 223–228. [CrossRef]
12. Yang, J.; Steinbrück, M.; Tang, C.; Große, M.; Liu, J.; Zhang, J.; Yun, D.; Wang, S. Review on Chromium Coated Zirconium Alloy Accident Tolerant Fuel Cladding. *J. Alloys Compd.* **2022**, *895*, 162450. [CrossRef]
13. Liu, J.; Tang, C.; Steinbrück, M.; Yang, J.; Stegmaier, U.; Große, M.; Yun, D.; Seifert, H.J. Transient experiments on oxidation and degradation of Cr-coated Zircaloy in steam up to 1600 °C. *Corros. Sci.* **2021**, *192*, 109805. [CrossRef]
14. Meschter, P.J.; Opila, E.J.; Jacobson, N.S. Water Vapor—Mediated Volatilization of High-Temperature Materials. *Annu. Rev. Mater. Res.* **2013**, *43*, 559–588. [CrossRef]
15. Saunders, S.R.J.; Monteiro, M.; Rizzo, F. The oxidation behaviour of metals and alloys at high temperatures in atmospheres containing water vapour: A review. *Prog. Mater. Sci.* **2008**, *53*, 775–837. [CrossRef]
16. Pan, Y. Cr concentration driving the structural, mechanical, and thermodynamic properties of Cr-Al compounds from first-principles calculations. *Int. J. Quantum Chem.* **2019**, *119*, 1–10. [CrossRef]
17. Zhu, H.; Liu, H.; Huang, F.; Yi, J.; Ge, F. Effect of Cr/Al Atomic Ratio on the Oxidation Resistance in 1200 °C Steam for the CrAlSiN Coatings Deposited on Zr Alloy Substrates. *JOM* **2019**, *71*, 4839–4847. [CrossRef]
18. Weinberger, C.R.; Thompson, G.B. Review of phase stability in the group IVB and VB transition-metal carbides. *J. Am. Ceram. Soc.* **2018**, *101*, 4401–4424. [CrossRef]
19. Barsoum, M.W. The MN+1AXN phases: A new class of solids; thermodynamically stable nanolaminates. *Prog. Solid State Chem.* **2000**, *28*, 201–281. [CrossRef]
20. Eklund, P.; Beckers, M.; Jansson, U.; Högberg, H.; Hultman, L. The Mn+1AXn phases: Materials science and thin-film processing. *Thin Solid Films* **2010**, *518*, 1851–1878. [CrossRef]
21. Barsoum, M.W.; Radovic, M. Elastic and Mechanical Properties of the MAX Phases. *Annu. Rev. Mater. Res.* **2011**, *41*, 195–227. [CrossRef]
22. Tallman, D.J.; Anasori, B.; Barsoum, M.W. A Critical Review of the Oxidation of Ti2AlC, Ti3AlC2 and Cr2AlC in Air. *Mater. Res. Lett.* **2013**, *1*, 115–125. [CrossRef]
23. Zhang, J.; Tian, Z.; Zhang, H.; Zhang, L.; Wang, J. On the chemical compatibility between Zr-4 substrate and well-bonded Cr2AlC coating. *J. Mater. Sci. Technol.* **2019**, *35*, 1–5. [CrossRef]
24. Ougier, M.; Michau, A.; Lomello, F.; Schuster, F.; Maskrot, H.; Schlegel, M.L. High-temperature oxidation behavior of HiPIMS as-deposited Cr–Al–C and annealed Cr2AlC coatings on Zr-based alloy. *J. Nucl. Mater.* **2020**, *528*, 151855. [CrossRef]

25. Tang, C.; Grosse, M.K.; Trtik, P.; Steinbrück, M.; Stüber, M.; Seifert, H.J. H2 permeation behavior of Cr2AlC and Ti2AlC MAX phase coated Zircaloy-4 by neutron radiography. *Acta Polytech.* **2018**, *58*, 69–76. [CrossRef]

26. Imtyazuddin, M.; Mir, A.H.; Tunes, M.A.; Vishnyakov, V.M. Radiation resistance and mechanical properties of magnetron-sputtered Cr2AlC thin films. *J. Nucl. Mater.* **2019**, *526*, 151742. [CrossRef]

27. Tunes, M.A.; Imtyazuddin, M.; Kainz, C.; Pogatscher, S.; Vishnyakov, V.M. Deviating from the pure MAX phase concept: Radiation-tolerant nanostructured dual-phase Cr2AlC. *Sci. Adv.* **2021**, *7*, eabf6771. [CrossRef]

28. Mráz, S.; Tyra, M.; Baben, M.; Hans, M.; Chen, X.; Herrig, F.; Lambrinou, K.; Schneider, J.M. Thermal stability enhancement of Cr2AlC coatings on Zr by utilizing a double layer diffusion barrier. *J. Eur. Ceram. Soc.* **2019**, *40*, 1119–1124. [CrossRef]

29. Wang, Z.; Ma, G.; Liu, L.; Wang, L.; Ke, P.; Xue, Q.; Wang, A. High-performance Cr2AlC MAX phase coatings: Oxidation mechanisms in the 900–1100 °C temperature range. *Corros. Sci.* **2020**, *167*, 108492. [CrossRef]

30. Tang, C.; Große, M.; Ulrich, S.; Klimenkov, M.; Jäntsch, U.; Seifert, H.J.; Stüber, M.; Steinbrück, M. High-temperature oxidation and hydrothermal corrosion of textured Cr2AlC-based coatings on zirconium alloy fuel cladding. *Surf. Coat. Technol.* **2021**, *419*, 127263. [CrossRef]

31. Nam, C.; Choi, B.K.; Lee, M.H.; Jeong, Y.H. Creep strength of Zircaloy-4 cladding depending on applied stress and annealing temperature. *J. Nucl. Mater.* **2002**, *305*, 70–76. [CrossRef]

32. Limbäck, M.; Andersson, T. A Model for Analysis of the Effect of Final Annealing on the In- and Out-of-Reactor Creep Behavior of Zircaloy Cladding. In *Zirconium in the Nuclear Industry: Eleventh International Symposium*; Bradley, E.R., Sabol, G.P., Eds.; ASTM International: West Conshohocken, PA, USA, 1996; pp. 448–468. ISBN 978-0-8031-5343-1.

33. Tang, C.; Steinbrück, M.; Klimenkov, M.; Jäntsch, U.; Seifert, H.J.; Ulrich, S.; Stüber, M. Textured growth of polycrystalline MAX phase carbide coatings via thermal annealing of M/C/Al multilayers. *J. Vac. Sci. Technol. A* **2020**, *38*, 013401. [CrossRef]

34. Tang, C.; Steinbrueck, M.; Stueber, M.; Grosse, M.; Yu, X.; Ulrich, S.; Seifert, H.J. Deposition, characterization and high-temperature steam oxidation behavior of single-phase Ti2AlC-coated Zircaloy-4. *Corros. Sci.* **2018**, *135*, 87–98. [CrossRef]

35. Oliver, W.C.; Pharr, G.M. Measurement of hardness and elastic modulus by instrumented indentation: Advances in understanding and refinements to methodology. *J. Mater. Res.* **2004**, *19*, 3–20. [CrossRef]

36. Oliver, W.C.; Pharr, G.M. An improved technique for determining hardness and elastic modulus using load and displacement sensing indentation experiments. *J. Mater. Res.* **1992**, *7*, 1564–1583. [CrossRef]

37. Tang, C.; Klimenkov, M.; Jaentsch, U.; Leiste, H.; Rinke, M.; Ulrich, S.; Steinbrück, M.; Seifert, H.J.; Stueber, M. Synthesis and characterization of Ti2AlC coatings by magnetron sputtering from three elemental targets and ex-situ annealing. *Surf. Coat. Technol.* **2017**, *309*, 445–455. [CrossRef]

38. Musil, J. Hard nanocomposite coatings: Thermal stability, oxidation resistance and toughness. *Surf. Coat. Technol.* **2012**, *207*, 50–65. [CrossRef]

39. Bull, S.J. Failure modes in scratch adhesion testing. *Surf. Coat. Technol.* **1991**, *50*, 25–32. [CrossRef]

40. Hajas, D.E.; Baben, M.; Hallstedt, B.; Iskandar, R.; Mayer, J.; Schneider, J.M. Oxidation of Cr2AlC coatings in the temperature range of 1230 to 1410 °C. *Surf. Coat. Technol.* **2011**, *206*, 591–598. [CrossRef]

41. Lin, Z.; Zhou, Y.; Li, M. Synthesis, microstructure, and property of Cr2AlC. *J. Mater. Sci. Technol.* **2007**, *23*, 721–746.

42. Chong, X.Y.; Jiang, Y.H.; Zhou, R.; Feng, J. Multialloying effect on thermophysical properties of Cr7C3-type carbides. *J. Am. Ceram. Soc.* **2017**, *100*, 1588–1597. [CrossRef]

43. Jiang, J.; Zhan, D.; Lv, J.; Ma, X.; He, X.; Wang, D.; Hu, Y.; Zhai, H.; Tu, J.; Zhang, W.; et al. Comparative study on the tensile cracking behavior of CrN and Cr coatings for accident-tolerant fuel claddings. *Surf. Coat. Technol.* **2021**, *409*, 126812. [CrossRef]

44. Stueber, M.; Holleck, H.; Leiste, H.; Seemann, K.; Ulrich, S.; Ziebert, C. Concepts for the design of advanced nanoscale PVD multilayer protective thin films. *J. Alloys Compd.* **2009**, *483*, 321–333. [CrossRef]

45. Tang, C.; Steinbrück, M.; Grosse, M.; Ulrich, S.; Seifert, H.J.; Stüber, M. Development of Cr-C-Al based coatings for enhanced accident tolerance fuel (ATF) cladding. In Proceedings of the Topfuel2021, Santander, Spanien, 24–28 October 2021; pp. 1–10.